Journal of Applied Electrochemistry **34**: 225–233, 2004.

Voltammetric and Raman microspectroscopic studies on artificial copper pits grown in simulated potable water

A.G. CHRISTY[1], A. LOWE[2], V. OTIENO-ALEGO[3,†], M. STOLL[2] and R.D. WEBSTER[4,*]
[1]*Department of Geology, Australian National University, Canberra ACT 0200, Australia*
[2]*Department of Engineering, Australian National University, Canberra ACT 0200, Australia*
[3]*Division of Science and Design, University of Canberra, Canberra ACT 2601, Australia*
[4]*Research School of Chemistry, Australian National University, Canberra ACT 0200, Australia*
[†]*Present address: Forensic Services, Australian Federal Police, GPO Box 401, Canberra ACT 2601, Australia*
*(*author for correspondence, fax: +61-2-6125-0750, e-mail: webster@rsc.anu.edu.au)*

Received 27 May 2003; accepted in revised form 27 August 2003

Keywords: bicarbonate ions, chloride ions, copper corrosion, pitting corrosion, potable water, Raman microspectroscopy, sulphate ions

Abstract

Artificial copper pits were prepared by electrochemically oxidising 60–80 μm diameter copper wires embedded in an epoxy resin over periods of 12–14 h. The electrolyte matrix consisted of various combinations of approximately 40 ppm unbuffered solutions (pH = 6–8) of sodium salts of Cl^-, HCO_3^- and SO_4^{2-} that are similar in concentration to what are found in potable water supplies in many metropolitan areas throughout the world. It was found that in the concentrations used for the study, HCO_3^- and to a lesser degree Cl^- had a positive affect on preventing pit growth under potentiostatic control, with both anions causing passivation of the copper metal. On the other hand, SO_4^{2-} was found to be very aggressive to copper dissolution and led to the formation of relatively deep pits (about 0.5 mm). Raman microspectroscopic analyses were performed on the freshly prepared undried caps that formed at the top of the pits and allowed the identification of several corrosion products by a comparison with standard copper mineral samples. The most complicated cap structure was observed in the presence of all three anions with distinct regions of the pit corresponding to cuprite (Cu_2O), eriochalcite ($CuCl_2 \cdot 2H_2O$), atacamite and/or botallackite [$Cu_2Cl(OH)_3$] and brochantite [$Cu_4(SO_4)(OH)_6$].

1. Introduction

Passive films formed on copper electrodes in neutral or basic solutions have a duplex structure with an outer layer of CuO or $Cu(OH)_2$ (depending on the electrode potential) and an inner layer of Cu_2O [1–8]. Aqueous solutions containing either carbonate or phosphate have been shown to improve the protective coating of the copper oxide/hydroxide layers [9–14], with *ex situ* X-ray photoelectron spectroscopy (XPS) experiments of copper surfaces placed in carbonate–bicarbonate solutions favouring the formation of copper carbonate species of uncertain identities [14]. The formation of thermodynamically and kinetically stable passive films in approximately neutral pH media is the principal chemical reason (in addition to economic and engineering considerations) that copper tubes are a widely used and generally reliable conduit for domestic water supplies. However, corrosion of copper in potable water can occur due to changes in the 'ideal' water composition resulting in classical Type 1 (cold water) [15, 16], Type 2 (hot water) [17] and Type 3 (soft water) pitting (Type 1 1/2 pitting has been coined to occur in situations involving microbially influenced corrosion processes of copper tubes [18]).

One source of pitting corrosion of copper is the presence of aggressive anions such as Cl^- and SO_4^{2-} [19–34], which accelerate the breakdown of the passive layers, although the aggressiveness of Cl^- has been questioned in the concentrations typically found in potable water [22–24]. Studies of pitting corrosion caused by SO_4^{2-} in the presence of HCO_3^- identified a critical breakdown potential that was related to both the absolute concentration of passive and aggressive anions and the ratio of HCO_3^- to SO_4^{2-} [20]. XPS and electrochemical studies examining the morphology and corrosion products of copper pits in Cl^- and SO_4^{2-} borate buffered solutions found a synergetic effect between the two supposedly aggressive anions [25, 26]. Pits generated in Cl^- solutions displayed an atacamite cap [$Cu_2Cl(OH)_3$] above a layer of CuCl while pits generated in sulphate solutions had a duplex structure of copper hydroxide and brochantite [$Cu_4(SO_4)(OH)_6$] above the base metal. Solutions of SO_4^{2-} were found to

be more aggressive to pit propagation than chloride since the CuCl layer formed in Cl^- solutions inhibited further metal dissolution. Solutions containing both Cl^- and SO_4^{2-} showed intermediate behaviour between the two extremes [25, 26].

Most studies utilising anodic oxidation to produce modified surface films on copper have been conducted at a relatively high concentration of aggressive or passive ions (>0.01 M). In this study we report experiments containing the anions SO_4^{2-}, Cl^- and HCO_3^- in the concentration range typically found in potable water supplies (20–200 ppm) [35]. The aim of the experiments is to identify copper corrosion products that are produced relatively quickly (within a few hours) on a very small scale, and compare the results with other reports over longer times and higher anion concentrations. The artificial copper pits were prepared by voltammetrically forcing dissolution of 60 or 80 μm copper wires embedded in an epoxy matrix which allowed controlled growth of the pit, similar to studies performed on stainless steel pits [36]. The morphology and chemical composition of the pit caps were examined by Raman spectroscopy. This technique is particularly useful for *in situ* studies because H_2O scatters only weakly between 3100 and 150 cm^{-1} [37]. Thus, the samples do not need to be dried (as required for SEM, EDX and XPS analysis) and there is reduced probability of alteration of the corrosion products prior to spectroscopic analysis. Raman spectroscopy has previously been used in corrosion related studies to examine the inhibition properties of benzotriazole and related compounds absorbed on copper [38], to identify passive films formed on copper [39–42] and to probe corrosion products formed on archaeological samples [43–47]. The Raman spectra of a collection of copper containing mineral samples of significance in corrosion have recently been reported and many of their important vibrational bands identified [48].

2. Experimental details

Copper electrodes were prepared by soldering 60 and 80 μm diameter commercial electrical copper wire (99.99%) onto 1 mm diameter copper wire and sealing the wires inside cylindrical Perspex tubes (10 mm *od* × 7 mm *id*) with Buehler Epoxide resin/hardener (Figure 1a). The end of the tubes were machined to expose the planar 60 or 80 μm diameter copper electrodes that were polished consecutively with P800 (21.8 μm) and P1200 (15.3 μm) grades of SiC paper followed by polishing with 800 (12.2 μm), 1200 (6.5 μm) and 1600 (3 μm) grit alumina oxide on Buehler Ultra-Pad polishing cloths. The Cu electrode was immersed facing upwards in a 400 cm^3 beaker with an Ag/AgCl reference electrode positioned to within 1 mm of the electrode surface (Figure 1b) with a Pt mesh auxiliary electrode completing the three-electrode circuit. In order to minimise the reference electrode filling solution

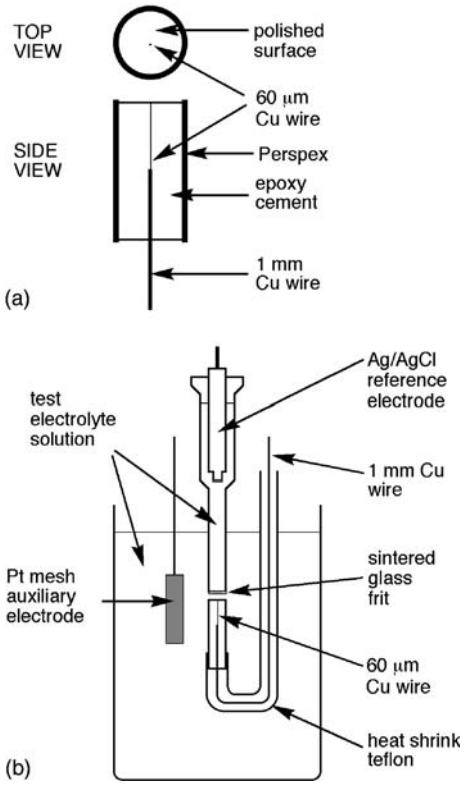

Fig. 1. Schematic diagram of (a) electrode and (b) electrochemical cell used for copper pitting experiments.

(saturated KCl) mixing with the low electrolyte concentration test solution, a salt bridge separating the two solutions was replenished between each experiment with an aliquot of the test solution. Controlled potential electrolysis and linear sweep voltammetry experiments were conducted with a PAR 273A potentiostat/galvanostat controlled through a PC with standard PAR software. Test solutions consisted of various mixtures of analytical grade NaCl, $NaHCO_3$ and Na_2SO_4 (20–200 ppm) in doubly distilled water.

Raman spectra were recorded using a Raman imaging microscope (Renishaw Plc, model 2000) coupled with an Olympus BH2 microscope. The Ramascope was equipped with an air-cooled CCD detector, a motorised XYZ stage and a CCD camera for video image viewing. A HeNe laser (632.8 nm) was used as the excitation source. The Ramascope was set-up in its confocal mode [49] in order to achieve a high spatial resolution (that is typically 1–1.5 μm). Integration times ranged between 20 and 40 s and 5–10 spectra were accumulated. The laser power was set to a low value (less than 6 mW) to avoid sample damage.

3. Results and discussion

3.1. *Cyclic voltammetry*

Cyclic voltammograms obtained at a scan rate of 2 mV s^{-1} using the 60 μm diameter copper wire elec-

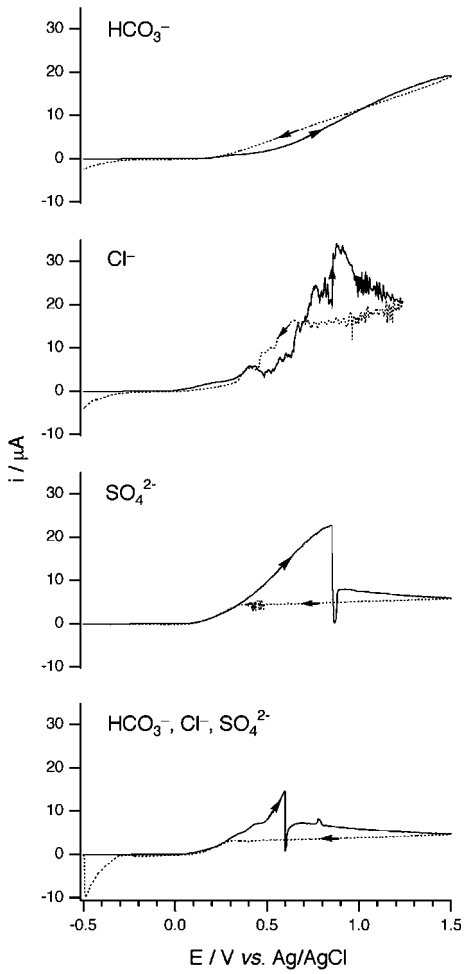

Fig. 2. Current–voltage curves obtained at a scan rate of 2 mV s^{-1} at 60 μm diameter copper wire electrodes in solutions containing 40 ppm of each individual anion and a mixture of all three anions. (—) Forward scan, (···) Reverse scan.

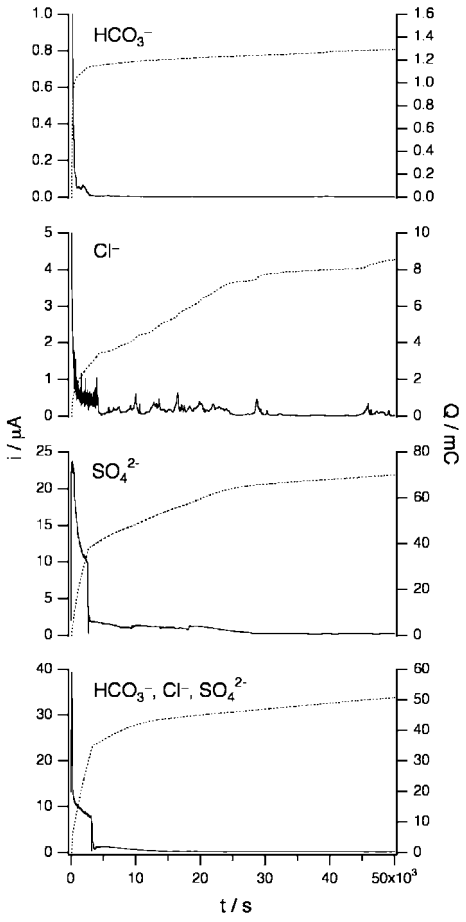

Fig. 3. (—) Current–time and corresponding (···) charge–time curves obtained during controlled potential electrolysis at 0.6 V vs Ag/AgCl at 60 μm diameter copper electrodes in solutions containing 40 ppm of each individual anion and a mixture of all three anions.

trodes in 40 ppm bicarbonate, chloride and sulphate solutions are displayed in Figure 2. Using very low electrolyte concentrations resulted in a substantial ohmic resistance contribution to the voltammetric data. Even though small electrodes were used (resulting in small corrosion currents), it can be estimated from the specific conductivity of the solutions that the iR_u drop is likely to be as high as 0.5 V, leading to substantially drawn out voltammograms.

In solutions containing only HCO_3^-, the voltammetric scan showed a gradual increase in current at about +0.25 V that progressively increased as the potential was scanned up to +1.5 V. Using the same solution and a substantially larger Pt electrode (1 mm diameter) the current obtained during CV experiments did not rise above 1 μA. Therefore, it can be concluded that the current that is observed at positive potentials at a Cu electrode is not due to background faradaic processes (but rather due to processes associated with the oxidation of Cu).

In solutions containing Cl^- the current response at positive potentials was very irregular, suggestive of numerous micro-scale passivation events occurring during the oxidation process. A peak maximum was usually observed between 0.7 and 1.0 V (Figure 2).

In SO_4^{2-} solutions, the voltammograms showed a smooth increase in current as the potential was increased until complete passivation of the electrode was observed (shown by the current rapidly diminishing to zero) typically occurring somewhere between 0.5 and 1.0 V. At higher potentials (or longer times) the current partially recovered suggesting further dissolution of the copper metal (Figure 2).

Solutions containing mixtures of all three anions (bottom curve in Figure 2) showed intermediate behaviour between that observed for each individual anion. For example, the overall current was diminished similar to that observed in the presence of only HCO_3^-, the current voltage trace was somewhat irregular as in the case of only Cl^-, and there was evidence of an event initiating complete passivation of the electrode surface such as that observed during oxidation of copper in the presence of only SO_4^{2-}.

3.2. *Controlled potential electrolysis*

Figure 3 shows current vs time and charge vs time curves obtained during the controlled potential oxidation

of the copper electrodes at 0.6 V in the presence of different electrolytes. While the short term (about 30 min) CV experiments shown in Figure 2 suggested that Cu metal could be oxidised when sufficiently positive potentials were applied in each of the three electrolytes, the controlled potential electrolysis experiments obtained over approximately 14 h (Figure 3) indicated that sustained oxidation resulting in substantial dissolution of solid Cu only occurred when sulphate was present.

In solutions containing only HCO_3^-, the current decayed to negligible amounts within about 1 h of the electrolysis commencing. Visually there was no evidence of any dissolution of the copper electrode.

In solutions containing only Cl^-, the current decreased quickly to <1 μA and remained irregular over the course of the experiment. While an appreciable charge could be measured at the completion of the experiment, microscopic inspection showed a relatively small amount of alteration/dissolution of the copper metal that penetrated to just a few microns depth. The controlled potential coulometry trace in Figure 3 indicates that the dissolution occurs via a metastable pitting process with periods of complete repassivation. Often, experiments that involved oxidation in the presence of chloride resulted in oscillatory current-potential behaviour suggesting that some of the measured current may be due to capacitance effects in addition to the pitting events.

In sulphate solutions, relatively high currents were obtained for at least the first hour of the electrolysis until a passivating event occurred (presumably salt film formation) which considerably slowed down or prevented further pit growth. The time at which the passivating event occurred was random, and largely determined the depth to which the pit would grow within the allotted time. For example, in some experiments the passivating event did not occur, that ultimately resulted in a very deep pit, whilst in other experiments the pit passivated within several minutes resulting in a much shallower pit after electrolysis for an equivalent amount of time. Increasing the applied potential between 0.6 and 0.8 V did not notably change the current–time behaviour.

Solutions containing mixtures of all three anions showed similar behaviour to that observed with sulfate only (Figure 3), indicating that SO_4^{2-} was the most important anion facilitating pit growth under controlled potential conditions.

Experiments were extended over a range of analyte concentrations in order to determine the effect of variable solution composition on the appearance of the cap above the pit mouth, the depth of the pit and the number of electrons transferred during growth of the pit (the data are summarised in Table 1). The pit depth (l/cm) was measured using an optical microscope which, when combined with knowledge of the charged passed (Q/A s), allowed the calculation of the number of electrons (n) transferred via

$$n = \frac{QM}{\pi r^2 l \rho F} \tag{1}$$

M is the molecular weight of Cu (63.54 g mol^{-1}), r is the radius of the electrode (0.003 or 0.004 cm), ρ is the density of Cu (8.9 g cm^{-3}) and F is the Faraday constant (96485 C mol^{-1}). The calculation assumes that all measured current is attributable to the dissolution of copper.

Table 1. Data associated with the controlled potential oxidation of 80 μm diameter copper electrodes at 0.6 V vs Ag/AgCl

Solution composition			pH[a]	Pit depth /mm[b]	Q /C (t/s)[c]	No. of electrons[d]	Cap/yes or no[e]
$[Cl^-]$/ppm	$[HCO_3^-]$/ppm	$[SO_4^{2-}]$/ppm					
40	0	0	5.8	Not detectable	0.009 (50 400)	?	Not detectable
0	40	0	8.0	Not detectable	0.001 (50 400)	?	Not detectable
0	0	40	6.0	0.51	0.057 (18 000)	1.66	Not detectable
20	20	0	7.7	Not detectable	0.011 (50 400)	?	Not detectable
20	60	0	7.9	Not detectable	0.006 (50 400)	?	Not detectable
60	20	0	7.4	Not detectable	0.012 (50 400)	?	Not detectable
20	0	20	6.1	0.43	0.056 (50 400)	1.92	Yes
20	0	60	5.6	0.51	0.067 (50 400)	1.93	Yes
60	0	20	5.7	0.63	0.081 (50 400)	1.89	Yes
200	0	20	5.7	0.17	0.022 (50 400)	1.86	No
0	20	20	7.7	0.25	0.031 (50 400)	1.88	Yes
0	20	60	7.6	0.54	0.067 (50 400)	1.83	Yes
0	60	20	8.0	0.67	0.086 (50 400)	1.89	Yes
0	200	20	8.2	0.45	0.059 (50 400)	1.93	Yes
20	20	20	7.7	0.30	0.035 (11 920)	1.72	Yes
20	20	20	7.5	0.56	0.068 (50 400)	1.79	Yes
20	60	20	7.9	0.25	0.033 (50 400)	1.95	Yes
20	20	60	7.9	0.32	0.045 (50 400)	1.99	Yes
60	20	20	7.3	0.31	0.042 (10 800)	1.99	Yes
60	60	20	8.0	0.42	0.051 (50 400)	1.78	Yes

[a] Measured prior to electrolysis; [b] measured with an optical microscope; [c] calculated by integrating current–time plots; [d] calculated using Equation 1 (see text); [e] determined by visual observation.

The test solutions were deliberately not buffered since such a process would necessarily introduce a high concentration of additional anions that would likely effect the composition of the pit caps. The pH of the unbuffered solutions (Table 1) was governed by the amount of dissolved CO_2 (which was not controlled) and the presence of bicarbonate. The addition of bicarbonate increased the pH from about 6 to about 8 due to its amphiprotic properties (Table 1) whilst Cl^- and SO_4^{2-} had no noticeable effect on the pH. There was no observable change in the pH of the solutions at the completion of the periods of pit growth. Studies have indicated that the pH inside the pit can be very acidic [50, 51], however, in this instance it appears that any increase in acidity caused by pit growth is not observable in the bulk solution due to the large dilution factor that occurs when ions diffuse from the pit.

In all cases where a pit of measurable depth was obtained (i.e. in sulphate containing solutions), the number of electrons transferred during the oxidation process was calculated to be 1.8 ± 0.2, suggesting that the dissolution largely proceeded by two electrons, or via Cu^{2+} rather than Cu^+ (Table 1). Solutions containing sulphate (in addition to other ions) almost all displayed a cap above the pit; the exceptions being in high chloride and low sulphate solutions and in pure sulphate only solutions where no caps were observed. Examining the pits under an optical microscope showed differences in the caps depending on the electrolyte composition. In solutions containing sulphate and chloride, red coloured crystalline material could be seen to cap the pit and was deposited on the polymer areas surrounding the artificial pit. In solutions containing sulphate and hydrogen carbonate, blue/green coloured crystals could be seen to make up the pit cap, with many blue/green crystals scattered around the pit mouth. Solutions containing all three anions produced mixtures of the scenarios described above.

Figure 4 shows a photograph of the side view of an artificial copper pit that was produced by oxidising a 60 μm copper wire embedded in an epoxy matrix. In this case the pit grew to a depth of about 0.5 mm over a period of 14 h. The lower two thirds of the pit appeared to be relatively free of detritus whilst the upper third displayed material that covered the inside walls of the pit, possibly even blocking the exit of material from the pit (the observation of an upper area containing detritus above a lower area free of detritus was typical of most of the pits investigated). It is possible that the rapid growth of the pit resulted in a high concentration of dissolved salts that subsequently precipitated out of solution before they could diffuse away from the pit mouth. Such a process would lead to an increase of the resistivity of the pit and could block the pit growth if electrical contact was sufficiently diminished between the working and auxiliary electrodes. The pit mouth showed a blue/green crystalline cap extending 50–100 μm above the pit with many crystals scattered around the mouth of the pit over a about 2 mm radius.

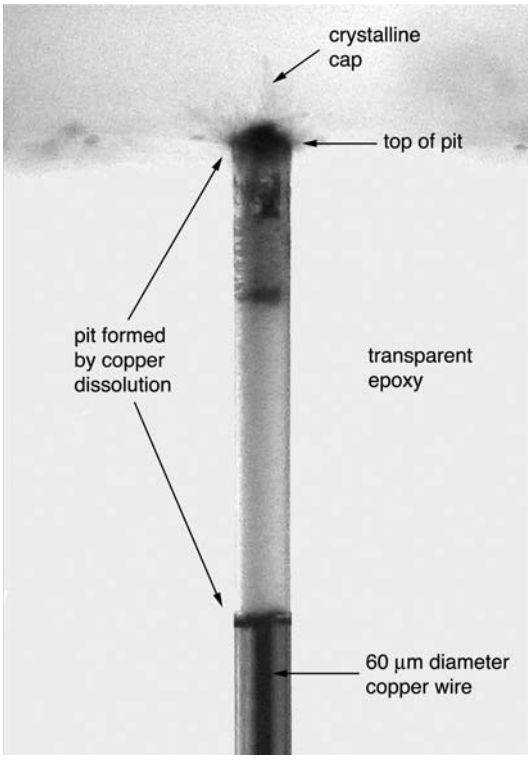

Fig. 4. Photograph taken through a microscope of the cross-section through an artificial copper pit grown potentiostatically (0.6 V vs Ag/AgCl) from a 60 μm copper wire embedded in an epoxy matrix for 14 h in a 40 ppm (each) solution of $NaHCO_3$, NaCl and Na_2SO_4. See 60 μm copper wire for scale.

3.3. *Raman microspectroscopy*

Raman microanalyses were undertaken immediately following the completion of pit growth. The electrodes were carefully rinsed with distilled water to remove excess electrolyte and the deposits constituting the cap were each pinpointed using the video viewer and the targeted species analysed by focussing the laser beam *via* the microscope objective (×50). Identification of the crystalline deposit was achieved by matching the Raman spectrum with those recorded for reference copper compounds. The reference copper minerals were selected by searching a mineral database [52] for species that contained one or more of the following ions; HCO_3^-, Cl^-, SO_4^{2-} and Na^+ (the sodium is present as the counterion for the electrolyte anions) and are listed in Table 2. Copper species containing additional ions were excluded from the table. The copper minerals that were used as reference standards came from a private collection of one of the authors (AGC), and where possible, the mineral spectra were cross checked with their commercially available forms, such as for the simple chloride and sulphate salts and the metal oxides. Carbonate containing minerals were excluded from Table 2 since it was believed that there would be a minimal amount of CO_3^{2-} derived from the bicarbonate at the pH range over which the experiments were conducted ($pH \leqslant 8$).

Table 2. Name and structure of copper containing minerals that contain a combination of one or more of Cl^-, SO_4^{2-} and Na^+ [a,b,c]

	Mineral Name	Formula	Crystal system	Standard available for comparison?
Copper chlorides	Anthonyite	$Cu(OH,Cl)_2 \cdot 3H_2O$	Monoclinic	No
	Atacamite	$Cu_2Cl(OH)_3$	Orthorhombic	Yes
	Belloite	$Cu(OH)Cl$	Monoclinic	No[e]
	Bobkingite	$Cu_5(OH)_8Cl_2 \cdot 2H_2O$	Monoclinic	No
	Botallackite	$Cu_2Cl(OH)_3$	Monoclinic	Yes
	Calumetite	$Cu(OH,Cl)_2 \cdot 2H_2O$	Orthorhombic	No
	Claringbullite	$Cu_4Cl(OH)_7$	Hexagonal	Yes
	Clinoatacamite	$Cu_2Cl(OH)_3$	Monoclinic	No
	Connellite[d]	$Cu_{19}Cl_4(SO_4)(OH)_{32} \cdot 2H_2O$	Hexagonal	Yes
	Eriochalcite	$CuCl_2 \cdot 2H_2O$	Orthorhombic	Yes
	Melanothallite	Cu_2OCl_2	Orthorhombic	No[e]
	Nantokite	$CuCl$	Cubic	Yes
	Paratacamite	$(Cu,Zn)_2Cl(OH)_3$	Trigonal	Yes
	Tolbachite	$CuCl_2$	Monoclinic	No[e]
Copper sulphates	Antlerite	$Cu_3(SO_4)(OH)_4$	Orthorhombic	Yes
	Bonattite	$CuSO_4 \cdot 3H_2O$	Monoclinic	No[e]
	Boothite	$CuSO_4 \cdot 7H_2O$	Monoclinic	No
	Brochantite	$Cu_4(SO_4)(OH)_6$	Monoclinic	Yes
	Chalcanthite	$CuSO_4 \cdot 5H_2O$	Triclinic	Yes
	Chalcocyanite	$CuSO_4$	Orthorhombic	No[e]
	Dolerophanite	$Cu_2(SO_4)O$	Monoclinic	No[e]
	Kröhnkite	$Na_2Cu(SO_4)_2 \cdot 2H_2O$	Monoclinic	Yes
	Langite	$Cu_4(SO_4)(OH)_6 \cdot 2H_2O$	Monoclinic	Yes
	Natrochalcite	$NaCu_2(SO_4)_2(OH,H_2O)_2$	Monoclinic	Yes
	Poitevinite	$CuSO_4 \cdot H_2O$	Monoclinic	No[e]
	Posnjakite	$Cu_4(SO_4)(OH)_6 \cdot H_2O$	Monoclinic	Yes
	Wroewolfeite	$Cu_4(SO_4)(OH)_6 \cdot 2H_2O$	Monoclinic	Yes
Copper oxides	Cuprite	Cu_2O	Cubic	Yes
	Paramelaconite	$Cu_2^{1+}Cu_2^{2+}O_3$	Tetragonal	No
	Tenorite	CuO	Monoclinic	Yes

[a] Table compiled from reference [52]; [b] minerals that contain additional anions or cations have been excluded; [c] there are no eligible minerals that contain bicarbonate; [d] connellite is the only mineral in the table that contains both chloride and sulfate; [e] unstable in contact with moist air and/or water.

For solutions containing only HCO_3^-, there was no pit growth and Raman microspectroscopy on the surface of the copper led to the detection of red Cu_2O (no bicarbonate containing species were detected). For solutions containing only sulphate, the copper electrode underwent complete dissolution in general, so a hole was detected in the epoxy matrix (Figure 5a). For solutions containing just chloride (Figure 5b), a red crystalline material was observed on top of the copper that extended a few microns above the pit (although the side view of the copper pits showed little dissolution had occurred). Raman microspectroscopy of the red material confirmed the presence of Cu_2O but no copper-chloride species were detected. However, the occurrence of a thin layer of CuCl directly above the base metal (as has been reported in high chloride concentration solutions [26]) may not be detectable with Raman microspectroscopy if it is completely covered by a layer of Cu_2O.

For solutions containing a mixture of bicarbonate and sulphate, the material making up the cap was composed of a mixture of Cu_2O and $CuSO_4 \cdot 5H_2O$ (chalcanthite) crystals. The appearance of water-soluble chalcanthite is indicative of a low pH regime or a very high concentration of copper sulfate. The role of HCO_3^- on the formation of the pit caps is interesting since no additional copper bicarbonate species were detected. It may be that the HCO_3^- simply acts to slow down the formation of the pit, or block the pit mouth by favouring the formation of Cu_2O, such that the pH inside the pit (or at the pit mouth) decreases to such a degree to cause the precipitation of chalcanthite.

The most pronounced effect on cap formation came in the presence of mixtures of Cl^- and SO_4^{2-} or in the presence of all three anions. Figure 5c represents a typical white light micrograph of the cap formed on top of the artificial pit generated by the oxidation of the copper wire in a solution containing HCO_3^-, Cl^- and SO_4^{2-}. The cap showed four distinct annular regions [marked (i)–(iv)]. The core of the cap consisted of red crystalline deposits (Figure 5c (i)] distributed within a matrix of very fine crystallites, nearly white in colour (Figure 5c (ii)]. Surrounding this core was an annular ring (Figure 5c (iii)] dominated by blue–green crystalline precipitates. The overall sizes of particles in region (iii) were larger than those observed within the core. The outer perimeter (Figure 5c (iv)] of the cap consisted of much larger, light-green, nearly transparent crystalline material.

Typical Raman spectra obtained for the different cap deposits obtained from the mixture HCO_3^-, Cl^- and

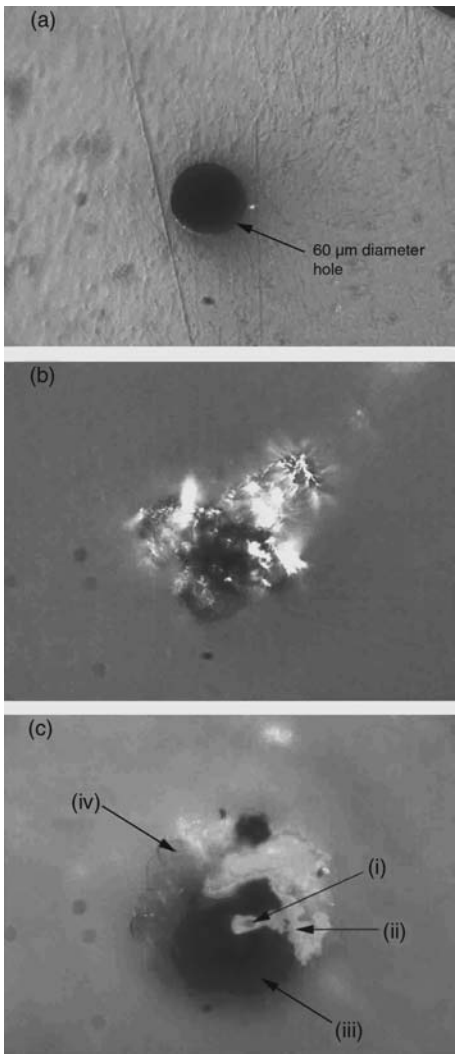

Fig. 5. Photographs taken through a microscope of the top of the pits that were grown potentiostatically (0.6 V vs Ag/AgCl) from a 60 μm copper wire embedded in an epoxy matrix for 14 h in a 40 ppm (each) solution of (a) Na_2SO_4, (b) NaCl and (c) $NaHCO_3$, NaCl and Na_2SO_4. See 60 μm hole in (a) for scale. (Photographs are the same scale.)

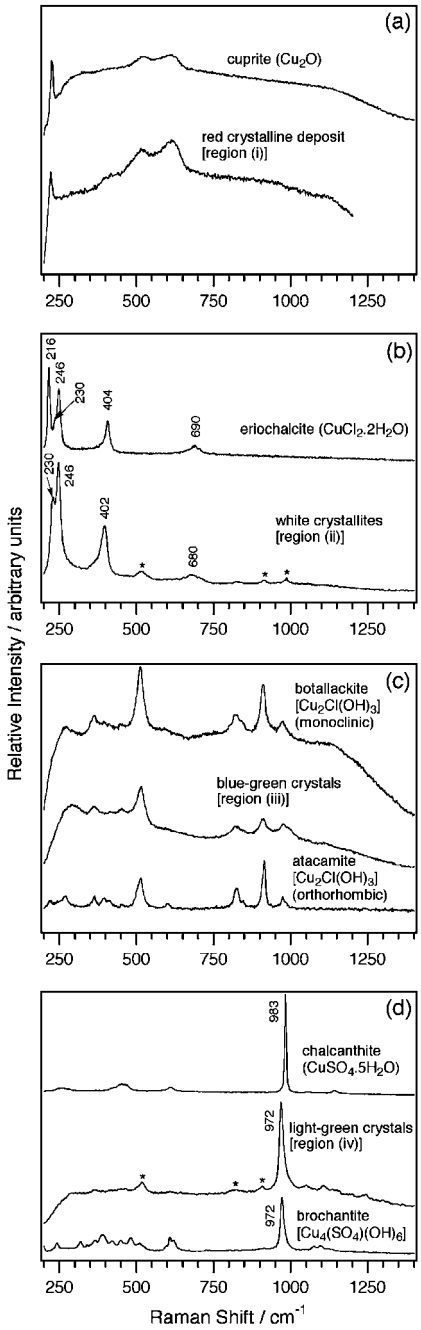

Fig. 6. Raman spectra of copper minerals in different regions of the pit cap [refer Figure 5c] that were grown potentiostatically (0.6 V vs Ag/AgCl) from a 60 μm copper wire embedded in an epoxy matrix for 14 h in a 40 ppm (each) solution of $NaHCO_3$, NaCl and Na_2SO_4. The associated mineral standards are included for comparison. $*$ = interference from botallackite crystals.

SO_4^{2-} together with the mineral reference spectra used for their identification are presented in Figure 6. The spectrum recorded for the pockets of red crystalline deposit present at the core of the cap was unambiguously identified to be cuprite (Cu_2O) (Figure 6a), the same as that observed in the presence of exclusively Cl^- or HCO_3^-. The spectra from the nearly white crystallites constituting region (ii) was very similar to that of eriochalcite ($CuCl_2 \cdot 2H_2O$), except for the peak at 216 cm^{-1} (Figure 6b). From the set of standard Raman spectra recorded, it was not possible to conclude whether this is the same $CuCl_2 \cdot 2H_2O$ species, with a slightly altered Raman spectrum being due to the very fine particle size, or if indeed it is a completely different copper chloride species. The spectrum was significantly different from that recorded for nantokite (CuCl), the other simple copper chloride that has been reported to form from chloride-sulfate containing solutions [26].

The Raman spectrum from the blue–green precipitates [(region (iii)] gave peaks at 280, 362, 515, 828, 912 and 981 cm^{-1} (Figure 6c) which were very similar to the reference spectra of atacamite and botallackite, both minerals having the same chemical composition [$Cu_2Cl(OH)_3$] but different crystal structures (orthorhombic and monoclinic respectively). Paratacamite, another polymorph of this composition, has a rhombohedral crystal structure (Table 2) and a substantially different Raman spectrum [48]. Of the three minerals, atacamite

has most commonly been reported as a corrosion product on copper [23, 43].

The Raman signal from a number of the larger crystals on the outer border of the cap (Figure 6d) exhibited a strong band at 975 cm^{-1}, which can be attributed to the symmetric stretching vibration of a sulfate anion (SO_4^{2-}). This band position corresponds to the strong peak observed in brochantite [$Cu_4(SO_4)(OH)_6$]. The other copper sulphate species likely to be present is chalcanthite ($CuSO_4 \cdot 5H_2O$), however, its strong SO_4^{2-} stretching vibration is well removed from that observed for the cap perimeter deposits (982 vs 975 cm^{-1}) (see Figure 6d). Hence the outer crystals are most likely brochantite whose weaker Raman bands are obscured by signals arising from the overlaying traces of botallackite. Brochantite has been proposed to be a key mineral in copper pitting problems associated with potable water supplies [23]. The occurrence of brochantite and atacamite/botallackite together suggests a complex relationship between Cl^- and SO_4^{2-}, since no $Cu_2Cl(OH)_3$ phases were detected as a corrosion product in solutions containing exclusively chloride.

The conditions used in this study did not lead to detectable amounts of the Cu^{II} oxide or hydroxide [CuO and $Cu(OH)_2$] that have often been reported to form as an outer layer above the inner Cu^{I} oxide (Cu_2O) in buffered solutions. The most likely reason for this is that the chloride and sulfate anions react rapidly with the simple Cu^{II} oxide and/or hydroxide to form water-soluble $CuCl_2$ or $CuSO_4$ species. This is supported by the detection of precipitated $CuCl_2 \cdot 2H_2O$ and $CuSO_4 \cdot 5H_2O$ in samples where the copper was dissolving rapidly (i.e. when sulfate was present), due to the localised solubility at the pit mouth being exceeded. An *in situ* surface enhanced Raman spectroscopic study found that oxidised copper reacts immediately with chloride on cyclic voltammetric time-scales to form CuCl or $CuCl_2$ [42]. Longer time-scale experiments have shown that in pits grown naturally (without applied potentials) in high chloride and sulfate containing solutions, the outer CuO and $Cu(OH)_2$ layers were replaced with chloride and sulfate containing minerals (brochantite and atacamite) [26]. The CuO and $Cu(OH)_2$ layers were thought to react with sulfate and/or chloride to form water soluble species. Brochantite is then able to form from sulfate ions by direct reaction with the oxidised base metal or with the cuprous oxide layer.

$$4Cu^{2+} + SO_4^{2-} + 6H_2O \rightarrow Cu_4(SO_4)(OH)_6 + 6H^+ \quad (2)$$

$$2Cu_2O + SO_4^{2-} + 4H_2O \rightarrow Cu_4(SO_4)(OH)_6 + 2H^+ + 4e^- \quad (3)$$

Analogous reactions can be written to account for the formation of atacamite and/or botallackite in chloride containing solutions.

$$2Cu^{2+} + Cl^- + 3H_2O \rightarrow Cu_2Cl(OH)_3 + 3H^+ \quad (4)$$

$$Cu_2O + Cl^- + 2H_2O \rightarrow Cu_2Cl(OH)_3 + H^+ + 2e^- \quad (5)$$

4. Conclusions

The applied potential (E/V) induced corrosion of copper in low electrolyte concentration (about 40 ppm) media containing HCO_3^-, Cl^- and SO_4^{2-} over short times (several hours) formed corrosion products whose identities generally agreed with those found in higher concentration studies or in field studies over longer periods of time. The chloride containing mineral, atacamite (and/or botallackite) [$Cu_2Cl(OH)_3$] and the sulphate-containing chemical analogue, brochantite [$Cu_4(SO_4)(OH)_6$], were found to be the principal corrosion products over a layer of cuprite (Cu_2O) and probably eriochalcite ($CuCl_2 \cdot 2H_2O$).

Sustained oxidation that resulted in substantial pit growth was found to occur only when sulphate was present. Furthermore, the absence of significant quantities of corrosion products in solutions that contained exclusively sulphate suggested that water soluble species (such as simple copper sulphates) were being formed, thereby allowing unfettered egress of the copper ions from the pit and preventing the pit from becoming blocked. When chloride or bicarbonate were added to the sulfate solutions, voluminous corrosion products were detected at the mouth of the pit. Microscopy studies on the side views of the pit confirmed that there was extensive build up of corrosion products in the upper portions of the pit, as the pits grew deeper (when Cl^- and/or HCO_3^- were present). In solutions containing a mixture of bicarbonate and sulphate, chalcanthite was detected as a corrosion product at the mouth of the pit, which confirmed the formation of simple copper sulphates as corrosion products.

Solutions containing exclusively chloride (or chloride and bicarbonate) displayed metastable pitting before complete repassivation of the pit, in keeping with recent studies that have suggested that low concentrations of chloride act in a protective manner towards copper in potable water systems [23]. However, when sulphate or sulphate/bicarbonate solutions were combined with chloride anions, chloride-containing minerals were detected suggesting a complex synergistic relationship between chloride and sulphate.

Acknowledgements

RDW acknowledges financial support for this project from the Australian Research Council through the award of a QEII Fellowship. Colour versions of Figures 4 and 5 are available electronically by contacting RDW.

References

1. H.-H. Strehblow and B. Titze, *Electrochim. Acta* **25** (1980) 839.
2. H.-D. Speckmann, M.M. Lohrengel, J.W. Schultze and H.-H. Strehblow, *Ber Bunsenges. Phys. Chem.* **89** (1985) 392.
3. M.R.G. de Chialvo, R.C. Salvarezza, D. Vásquez Moll and A.J. Arvia, *Electrochim. Acta* **30** (1985) 1501.
4. M.R.G. de Chialvo, J.O. Zerbino, S.L. Marchiano and A.J. Arvia, *J. Appl. Electrochem.* **16** (1986) 517.
5. J. Gómez Becerra, R.C. Salvarezza and A.J. Arvia, *Electrochim. Acta* **33** (1988) 613.
6. C.I. Elsner, R.C. Salvarezza and A.J. Arvia, *Electrochim. Acta* **33** (1988) 1735.
7. M. Wanner, H. Wiese and K.G. Weil, *Ber Bunsenges. Phys. Chem.* **92** (1988) 736.
8. M. Drogowska, L. Brossard and H. Ménard, *Surf. Coat. Technol.* **34** (1988) 383.
9. M. Pérez Sánchez, M. Barrera, S. González, R.M. Souto, R.C. Salvarezza and A.J. Arvia, *Electrochim. Acta* **35** (1990) 1337.
10. M.M. Laz, R.M. Souto, S. González, R.C. Salvarezza and A.J. Arvia, *Electrochim. Acta* **37** (1992) 655.
11. M. Pérez Sánchez, R.M. Souto, M. Barrera, S. González, R.C. Salvarezza and A.J. Arvia, *Electrochim. Acta* **38** (1993) 703.
12. S.B. Ribotta, M.E. Folquer and J.R. Vilche, *Corrosion* **51** (1995) 682.
13. R.M. Souto, M.M. Laz and S. González, *An. Quim. Int. Ed.* **93** (1997) 252.
14. S. González, M. Pérez, M. Barrera, A.R. González Elipe and R.M. Souto, *J. Phys. Chem. B* **102** (1998) 5483.
15. H.S. Campbell, *J. Inst. Metals* **77** (1950) 345.
16. V.F. Lucey, *Br. Corros. J.* **2** (1967) 175.
17. E. Mattsson and A.M. Fredriksson, *Br. Corros. J.* **3** (1968) 246.
18. G.G. Geesey, P.J. Bremer, W.R. Fischer, D. Wagner, C.W. Keevil, J. Walker, A.H.L. Chamberlain and P. Angell, *in* G.G. Geesey, Z. Lewandowski and H.-C. Flemming, (Eds), 'Biofouling and Biocorrosion in Industrial Water Systems' (CRC Press, Boca Raton, Florida 1990), p. 243.
19. M. Drogowska, L. Brossard and H. Ménard, *J. Electrochem. Soc.* **139** (1992) 39.
20. I. Milošev, M. Metikoš-Huković, M. Drogowska, H. Ménard and L. Brossard, *J. Electrochem. Soc.* **139** (1992) 2409.
21. M. Drogowska, L. Brossard and H. Ménard, *J. Appl. Electrochem.* **24** (1994) 344.
22. M. Edwards and J.F. Ferguson, *Am. Water Works Assoc.* **85** (1993) 105.
23. M. Edwards, J.F. Ferguson and S.H. Reiber, *Am. Water Works Assoc.* **86** (1994) 74.
24. M. Edwards, J. Rehring and T. Meyer, *Corrosion* **50** (1994) 366.
25. J.P. Duthil, G. Mankowski and A. Giusti, *Corros. Sci.* **38** (1996) 1839.
26. G. Mankowski, J.P. Duthil and A. Giusti, *Corros. Sci.* **39** (1997) 27.
27. R.M. Souto, S. Gonzalez, R.C. Salvarezza and A.J. Arvia, *Electrochim. Acta* **39** (1994) 2619.
28. F.M. Alkharafi and H.M. Shalaby, *Corrosion* **51** (1995) 469.
29. R.E. Lobnig, R.P. Frankenthal, D.J. Siconolfi, J.D. Sinclair and M. Stratmann, *J. Electrochem. Soc.* **141** (1994) 2935.
30. M.E. Vela, G. Andreasen, S.G. Aziz, R.C. Salvarezza and A.J. Arvia, *Electrochim. Acta* **43** (1998) 3.
31. H. Strandberg and L.G. Johansson, *J. Electrochem. Soc.* **145** (1998) 1093.
32. K.P. Fitzgerald, J. Nairn and A. Atrens, *Corros. Sci.* **40** (1998) 2029.
33. S. Jouen, M. Jean and B. Hannoyer, *Surf. Interface Anal.* **30** (2000) 145.
34. A.G. Nord, K. Tronner and A.J. Boyce, *Water, Air, Soil Pollut.* **127** (2001) 193.
35. J.R. Dojlido and G.A. Best, *in* 'Chemistry of Water and Water Pollution' (Ellis Horwood, New York, 1993).
36. N.J. Laycock and R.C. Newman, *Corros. Sci.* **39** (1997) 1771.
37. R.S. Tobias, *in* A. Anderson (Ed.), 'The Raman Effect' (Marcel Dekker, New York, 1973), p. 408.
38. M. Metikoš-Huković, R. Babić and A. Marinović, *J. Electrochem. Soc.* **145** (1998) 4045.
39. C.A. Melendres, S. Xu and B. Tani, *J. Electroanal. Chem.* **162** (1984) 343.
40. J.C. Hamilton, J.C. Farmer and R.J. Anderson, *J. Electrochem. Soc.* **133** (1986) 739.
41. S.T. Mayer and R.H. Muller, *J. Electrochem. Soc.* **139** (1992) 426.
42. H.Y.H. Chan, C.G. Takoudis and M.J. Weaver, *J. Phys. Chem. B* **103** (1999) 357.
43. D.A. Scott, *Stud. Conserv.* **45** (2000) 39.
44. L. Burgio and R.J.H. Clark, *Spectrochem. Acta Part A* **57** (2001) 1491.
45. R.L. Frost, P.A. Williams, W. Martens and J.T. Kloprogge, *J. Raman Spectrosc.* **33** (2002) 752.
46. R.L. Frost, W. Martens, J.T. Kloprogge and P.A. Williams, *J. Raman Spectrosc.* **33** (2002) 801.
47. W. Martens, R.L. Frost, J.T. Kloprogge and P.A. Williams, *J. Raman Spectrosc.* **34** (2003) 145.
48. R.L. Frost, *Spectrochem. Acta Part A* **59** (2003) 1195.
49. K.P.J Williams, G.D. Pitt, D.N. Batchelder and B.J. Kip, *Appl. Spectrosc.* **48** (1994) 232.
50. B.E. Wilde and E. Williams, *Electrochim. Acta* **16** (1971) 1971.
51. T. Suzuki, M. Yamabe and Y. Kitamura, *Corrosion* **29** (1973) 70.
52. P. Perroud, *Athena Mineralogy* (http://un2sg4.unige.ch/athena/mineral/mineral.htm).